

Adversarial Fine-tuning for Backdoor Defense: Connecting Backdoor Attacks to Adversarial Attacks

Bingxu Mu¹, Zhenxing Niu², Le Wang¹, Xue Wang², Rong Jin², Gang Hua³

¹Xi'an Jiaotong University, ²Alibaba Group, ³Wormpex AI Research

Abstract—Deep neural networks (DNNs) are known to be vulnerable to both backdoor attacks as well as adversarial attacks. In the literature, these two types of attacks are commonly treated as distinct problems and solved separately, since they belong to training-time and inference-time attacks respectively. However, in this paper we find an intriguing connection between them: for a model planted with backdoors, we observe that its adversarial examples have similar *behaviors* as its triggered samples, *i.e.*, both activate the *same* subset of DNN neurons. It indicates that planting a backdoor into a model will significantly affect the model’s adversarial examples. Based on this observations, we design a new Adversarial Fine-Tuning (AFT) algorithm to defend against backdoor attacks. We empirically show that, against 5 state-of-the-art backdoor attacks, our AFT can effectively erase the backdoor triggers without obvious performance degradation on clean samples and significantly outperforms existing defense methods.

I. INTRODUCTION

Deep neural networks (DNNs) have been widely adopted in many real-world and safety-critical applications (*e.g.*, face recognition and autonomous driving), thus more attention has been paid to the security of deep learning. It has been demonstrated that DNNs are prone to potential threats in both their inference as well as training phases. Inference-time attack (known as *adversarial attack* [1], [2]) aims to fool a trained model into making incorrect predictions with small adversarial perturbations, a field that has been well-studied. In contrast, training-time attack (known as *backdoor attack* [3]) attempts to plant a backdoor into a model in the training phase, so that the infected model would misclassify testing samples as the *target-label* whenever a pre-defined *trigger* (*e.g.*, several pixels) is embedded into a testing sample.

In recent years, more and more attentions are brought to backdoor attacks. In order to fully utilize the power of the modern big DNNs, huge amount of training data and computing resources are required [4]–[6]. Therefore, in real-world applications, people tend to adopt third-party datasets or models, rather than to collect the training data or train the models by themselves. As a result, such outsourced scenarios increase the risk for an untrustworthy third-party to poison training data or plant backdoors. Lately, the study of the backdoor attack has made a significant progress [3], from visible to invisible trigger designs [7], [8], from poisoning-label to clean-label strategies [9]–[12].

The defense against backdoor attacks is more challenging and less studied. Specifically, in recent backdoor attacks, triggers are designed to be invisible to humans [8], [10], [13], meanwhile the ground-truth label of poisoned samples could also be consistent with the target label [9]. Both of them will

increase the stealthiness of backdoor attacks. As a result, it is very hard, even for the recent state-of-the-art defense methods, to detect poisoned samples or to erase backdoor from infected models [14]–[22]. Moreover, all previous defense methods require an additional clean dataset, which is often unavailable in realistic scenarios.

On the other hand, to our best knowledge, backdoor attacks and adversarial attacks are often treated as two different problems and solved separately in the literature. They intuitively are very different from each other since they belong to two distinct categories of attacks, *i.e.*, one belongs to training-time attacks while the other belongs to inference-time attacks. However, in this paper we show an underlying connection between them, and they potentially affect each other when we consider them simultaneously.

We find an intriguing connection between those two types of attacks: for a model planted with backdoors, we observe that its adversarial examples have similar *behaviors* as its triggered samples. It indicates that planting a backdoor into a model will significantly affect the model’s adversarial examples. Furthermore, based on such underlying connections we design a new Adversarial Fine-Tuning (AFT) algorithm to defend against backdoor attacks.

In particular, for a benign model, the predicted class labels of its adversarial examples obey a *uniform* distribution, as shown in Fig.1(a). However, **for an infected model, we surprisingly observe that its adversarial examples are highly likely classified as the backdoor target-label, which is the same as the behaviors of triggered samples**, as shown in Fig.1(b) and Fig.1(c). Particularly, these phenomena are present regardless of what target-labels are, what dataset is, what kinds of backdoor attacks are, and what trigger embedding functions are.

To find the underlying reason of such phenomena, we visualize and measure the similarity of the features of adversarial examples and triggered samples. We find that after planting a backdoor into one model, the features of adversarial examples change significantly. As illustrated in Fig.2, before planting a backdoor (*i.e.*, with benign models) the adversarial example \tilde{x} could fall in *any* class (*e.g.*, close to Class 0 or Class 2). But **after planting a backdoor** (*i.e.*, with infected models), the features of \tilde{x}' are surprisingly very similar to the features of triggered image x^t , and hence the \tilde{x}' will *highly likely* fall in the backdoor target-label class (*e.g.*, close to Class l). The similarity of features indicates that **both the \tilde{x}' and x^t have similar behaviors, *i.e.*, both activate the same subset of DNN neurons**.

Based on such underlying connections we design a simple

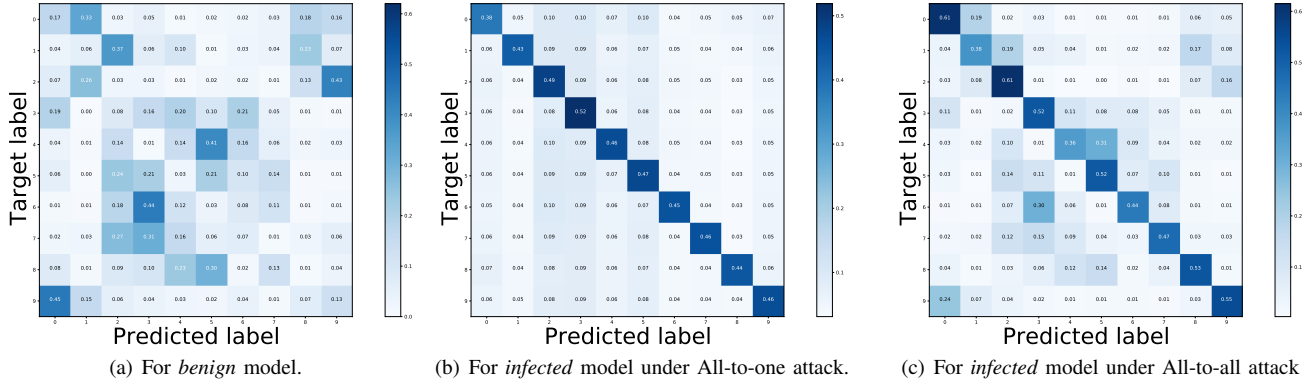


Fig. 1: Predicted labels v.s. Target-labels for 10,000 randomly sampled adversarial examples from CIFAR-10, with respect to *benign* and *infected* models. (a) For a benign model, the predicted labels obey *uniform* distribution; (b,c) for infected models under both All-to-one and All-to-all backdoor attacks (WaNet), its adversarial examples are *highly likely* classified as the target-label, as shown by the matrix diagonals.

but effective algorithm to defend against backdoor attacks. Specifically, our approach first generates adversarial examples for the infected model, and then we adversarially fine-tune the infected model with the generated adversarial examples. We call our approach *adversarial fine-tuning* (AFT) since we fine-tune the infected model with adversarial examples instead of clean samples. Since adversarial examples come from all image classes, our AFT performs like associating triggered samples to all image classes instead of just the target class, which breaks the foundation of backdoor attacks (*i.e.*, building a strong correlation between a trigger pattern and a target-label [17]). Hence our approach can achieve a defensive effect.

We also find that our approach has a promising defensive effect even **when the additional clean dataset is unavailable**. In this case, we assume that the poisoned training data is known, and we use them to generate adversarial examples. By using an early stop scheme, our approach maintains effective defensive performance even for a large poisoning ratio.

Our main contributions are summarized as follows:

- We observe an underlying connection between backdoor attacks and adversarial attacks, *i.e.*, for an infected model, its adversarial examples have similar behaviors to its triggered samples.
- According to the observation, we propose a simple but effective backdoor defense approach, which not only achieves the state-of-the-art defense performance but also has a defensive effect when an additional clean dataset is unavailable.

II. RELATED WORK

Backdoor Attack. The backdoor attack is a type of training-time attacks [7]. It first defines a trigger pattern, a target-label, and designs an embedding mechanism. A small subset of training data are then poisoned, *i.e.*, clean images are embedded with a trigger meanwhile their labels are replaced with the target-label. At last, an infected model can be obtained by training with the poisoned training data.

These trigger patterns can appear in forms as simple as a single pixel or a small patch [23], where the embedding mechanism is to directly add triggers into images. Next, more complex triggers such as sinusoidal strips [9] and blended patterns [23] are proposed. Recently, in order to make triggers more stealthy and hard to be detected even by humans, complex trigger-embedding mechanisms are proposed, such as input-aware dynamic patterns [13], natural reflection [10] and image warping [8]. A survey of backdoor attacks can be found in [3].

Backdoor Defense. Backdoor defense methods can be roughly categorized into backdoor detection and backdoor erasing. Detection-based methods aim at identifying the existence of backdoor in the underlying model [24], [25] or filtering the suspicious samples in training data for re-training [26]–[28]. Although they perform fairly well in distinguishing whether a model has been poisoned, the backdoor still remains in the infected model.

The erasing-based methods aim to directly purify the infected model by removing the malicious impacts caused by the backdoor triggers, while maintaining the model performance on clean data. One approach is to directly fine-tune the infected model with the additional clean dataset [14]. Fine-Pruning [15] proposes using neural pruning to remove backdoor neurons. Later, Neural Attention Distillation (NAD) [17] is proposed. But most of these methods can be evaded by advanced modern backdoor attacks [8], [10], [13]. Moreover, all previous defense methods need an additional clean dataset.

Another related work is the Neural Cleanse (NC) [24], which is also proposed for defence against backdoor attack. However, there are big differences between them. First, NC focuses on recovering the trigger. The recovered trigger is then used to make a defence. Therefore, NC can only handle *fix trigger* attack (*i.e.*, Badnet) instead of *dynamic trigger* attack (*i.e.*, DynamicAtt, WaNet). Second, recovering trigger at *pixel* space is unnecessary for making a defence, which restricts the application of NC. In contrast, our approach do not need to recover trigger at pixel space, but *generally* found the connection between triggered images and adversarial images at *feature* space. Thus, our observation is more general, and

our approach is more efficient to conduct defence.

Adversarial Attack and Defense. The adversarial attack [1], [2], [29]–[32] is a kind of inference-time attacks. It aims to fool a trained model into making incorrect predictions (*i.e.*, untargeted adversarial attack) or predicting the input as a particular label (*i.e.*, targeted adversarial attack).

On the other hand, many defense methods [33]–[40] are also proposed against adversarial attacks. *Adversarial training* [41] is one of the most effective methods. Recently, [42] proposes to use a ‘trapdoor’ to detect adversarial examples. It illustrates that a particular trapdoor could lead to producing adversarial examples similar to trapdoors in the feature space, which aligns with our observation that adversarial examples could have similar features as triggered images. However, it is quite different from our work since it aims to detect adversarial examples while our approach aims to defend against backdoor attacks.

III. OUR APPROACH

A. Backdoor Attack

We focus on backdoor attacks on image classification. Let $D_{train} = \{(\mathbf{x}_i; y_i)\}_{i=1}^N$ be the clean training data and $f(\mathbf{x}; \theta)$ be the benign CNN model decision function with parameter θ .

For backdoor attack, we define or learn a trigger embedding function $\mathbf{x}^t = Trigger(\mathbf{x})$ which can convert a clean sample \mathbf{x}_i to a triggered/poisoned sample \mathbf{x}_i^t . Given a target-label l , we can poison a small part of training samples, *i.e.*, replace (\mathbf{x}_i, y_i) with (\mathbf{x}_i^t, l) , which produces poisoned training data D'_{train} . The training with D'_{train} results in the infected model $f(\mathbf{x}; \theta')$. Note that different attacks will define different trigger embedding functions $Trigger()$.

At testing time, if a clean input $(\mathbf{x}, y) \in D_{test}$ is fed to the infected model, it is supposed to be correctly predicted as y . In contrast, for a triggered sample \mathbf{x}^t , its prediction changes to the target-label l . Particularly, backdoor attacks can be divided into two categories according to the selection of target-labels: (1) All-to-one attack: the target-labels for all examples are set as l ; (2) All-to-all attack: the target-labels for different classes could be set differently, such as $y + 1$, *i.e.*,

$$\text{All-to-one attack: } \begin{cases} f(\mathbf{x}; \theta') = y; \\ f(\mathbf{x}^t; \theta') = l, \mathbf{x}^t = Trigger(\mathbf{x}) \end{cases} \quad (1)$$

$$\text{All-to-all attack: } \begin{cases} f(\mathbf{x}; \theta') = y; \\ f(\mathbf{x}^t; \theta') = y + 1, \mathbf{x}^t = Trigger(\mathbf{x}) \end{cases} \quad (2)$$

B. Backdoor Defense

We adopt a typical defense setting where the defender has an infected model $f(\mathbf{x}; \theta')$ as well as an additional clean dataset D_{ext} . The goal of the backdoor defense is to *erase* the backdoor trigger from the model while retaining the performance of the model on clean samples. In other words, we want to obtain a cleaned/purified model $f(\mathbf{x}; \theta^c)$ so as to:

$$\begin{cases} f(\mathbf{x}; \theta^c) = y; \\ f(\mathbf{x}^t; \theta^c) = y, \mathbf{x}^t = Trigger(\mathbf{x}) \end{cases} \quad (3)$$

C. Untargeted Adversarial Attack

Untargeted adversarial attack aims to find the best perturbation \mathbf{r} so that the adversarial examples $\tilde{\mathbf{x}} = \mathbf{x} + \mathbf{r}$ will be misclassified, *i.e.*, the loss $L(\tilde{\mathbf{x}}, y)$ is maximized with respect to \mathbf{r} , as follows:

$$\max_{\mathbf{r}} L(\tilde{\mathbf{x}}, y; \theta) \quad (4)$$

$$\text{s.t. } \|\mathbf{r}\|_p < \epsilon, \tilde{\mathbf{x}} = \mathbf{x} + \mathbf{r} \\ \tilde{\mathbf{x}} \in [0, 1]^d \quad (5)$$

Note that untargeted adversarial attack means that perturbed inputs $\tilde{\mathbf{x}}$ are only desired to be misclassified (*i.e.*, different from their original labels y as Eq.(4)), rather than being classified as a particular label (which is the goal of the *targeted adversarial attack*). Therefore, it has been observed that the predicted labels of $\tilde{\mathbf{x}}$ obey a uniform distribution across all classes.

D. Empirical Observation and Analysis

In this section, we will describe how we obtain the observation that **for an infected model, its adversarial examples have similar behaviors to its triggered samples**. Specifically, we first conduct an untargeted adversarial attack on the *infected* model $f(\mathbf{x}; \theta')$ to generate adversarial examples $\tilde{\mathbf{x}}'$ as follows:

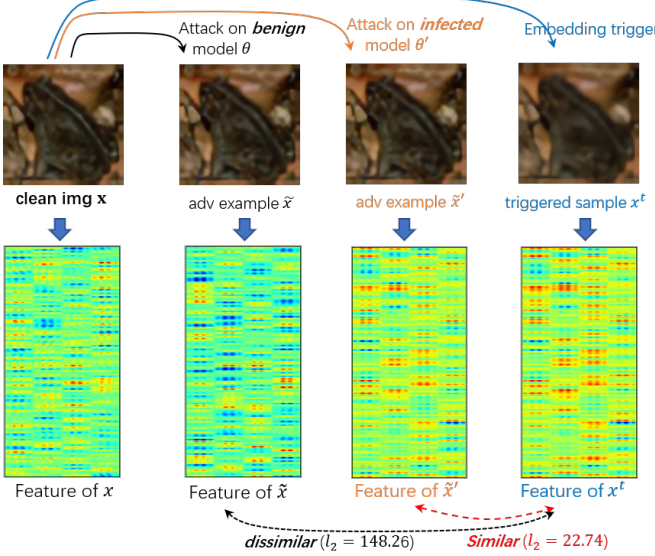
$$\max_{\mathbf{r}} L(\tilde{\mathbf{x}}', y; \theta') \quad (6)$$

$$\text{s.t. } \|\mathbf{r}\|_p < \epsilon, \tilde{\mathbf{x}}' = \mathbf{x} + \mathbf{r}$$

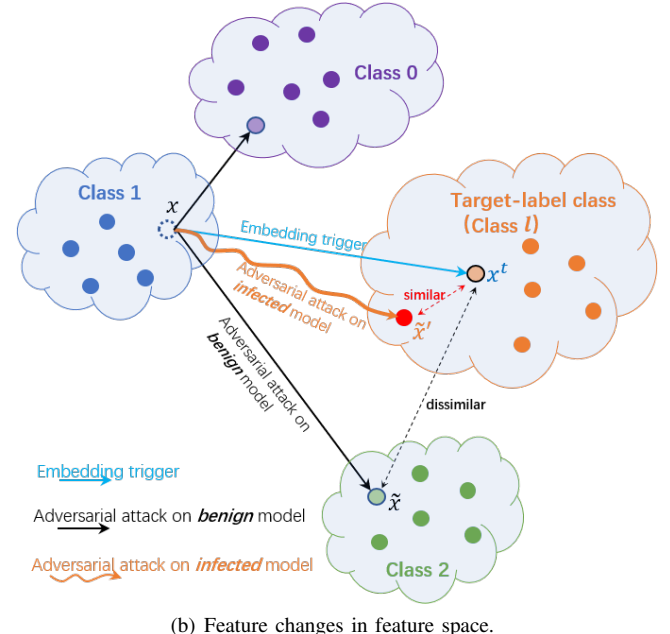
Meanwhile, we also conduct an untargeted adversarial attack on the *benign* model $f(\mathbf{x}; \theta)$ to produce the adversarial examples $\tilde{\mathbf{x}}$ as Sec.III-C.

We next examine the classification results of those adversarial examples. As shown in Fig.1(a), when feeding adversarial examples $\tilde{\mathbf{x}}$ to the benign model, $\tilde{\mathbf{x}}$ will be classified as any class with the same probability (except its ground-truth label), *i.e.*, obeying a uniform distribution. In contrast, as feeding adversarial examples $\tilde{\mathbf{x}}'$ to the infected model, we observe that $\tilde{\mathbf{x}}'$ are **highly likely classified as the target-label**. As shown in Fig.1(b) and 1(c), if an untargeted adversarial attack is conducted on an infected model with target-label $l \in \{0, \dots, 9\}$, we observe that at least more than 40% of $\tilde{\mathbf{x}}'$ are predicted as the target-label l . These phenomena are present regardless of what kinds of backdoor attack are and what dataset is, as shown in Fig.4.

It indicates that there is an underlying connection between adversarial examples $\tilde{\mathbf{x}}'$ and triggered samples \mathbf{x}^t , since \mathbf{x}^t are **also expected to be classified as the target-label**. For further investigation, we check the feature maps of clean samples \mathbf{x} , benign model’s adversarial examples $\tilde{\mathbf{x}}$, infected model’s adversarial examples $\tilde{\mathbf{x}}'$, and triggered images \mathbf{x}^t . We find that the features of $\tilde{\mathbf{x}}'$ are very similar to the features of triggered samples \mathbf{x}^t , while there is a significant difference between the features of $\tilde{\mathbf{x}}$ and \mathbf{x}^t . As shown in Fig.2(a), the l_2 distance between the features of $\tilde{\mathbf{x}}'$ and \mathbf{x}^t is smaller than that between $\tilde{\mathbf{x}}$ and \mathbf{x}^t . More quantitative comparisons can be seen in Table.I. Such feature similarity indicates that both adversarial examples $\tilde{\mathbf{x}}'$ and triggered samples \mathbf{x}^t could activate the *same* subset of DNN neurons, *i.e.*, **the adversarial**



(a) Feature maps of an example.



(b) Feature changes in feature space.

Fig. 2: The similarity of features for clean image x , benign model’s adversarial example \tilde{x} , infected model’s adversarial example \tilde{x}' , and triggered image x^t . Obviously, the features of \tilde{x}' are very similar to x^t . In contrast, there is a significant difference between the features of \tilde{x}' and \tilde{x} , which indicates adversarial examples will change significantly *after* planting a backdoor into a model.

examples \tilde{x}' have similar behaviors to triggered samples x^t .

We speculate why adversarial examples would have significant changes after a backdoor is planted into a model as follows: some DNN neurons will be activated by a trigger when a backdoor is planted into a model, which are called ‘backdoor neurons’. When conducting an adversarial attack on infected models, those ‘backdoor neurons’ are more likely to be chosen/locked and activated as generating adversarial examples. Thus, the generated adversarial examples could work like triggered samples. Furthermore, we have **theoretically justified** our observations for a linear model, as shown in the Sec V.

E. Adversarial Fine-tuning

Based on the previous observation, we propose an adversarial fine-tuning defense method. As shown in **Algorithm 1**, we first conduct an untargeted adversarial attack to generate adversarial examples from the clean images with the given infected model. Next, we adversarially fine-tune the infected model with those adversarial examples. At last, we find that the purified model could be further improved by normal fine-tuning (*i.e.*, fine-tuning with clean data). Note that stage-3 aims to improve ACC after erasing the backdoor, which is optional.

Specifically, given the infected model $f(x; \theta')$, for each $(x_i, y_i) \in D_{ext}$, we obtain a corresponding adversarial example \tilde{x}'_i according to Eq.(6), which produces $\tilde{D}_{ext} = \{\tilde{x}'_i, y_i\}_{i=1}^m$. And then, we fine-tune the infected model θ'

Algorithm 1 Adversarial Fine-tuning

Input: Infected model θ' , an additional clean dataset D_{ext}
Output: Purified model θ^c (or Advanced model θ^{c+})

- 1: Stage-1: untargeted adversarial attack
- 2: **for** $(x_i, y_i) \in D_{ext}$ **do**
- 3: Get adversarial example \tilde{x}'_i according to Eq.(6)
- 4: Obtain $\tilde{D}_{ext} = \{\tilde{x}'_i, y_i\}_{i=1}^m$
- 5: Stage-2: adversarial fine-tuning
- 6: **for** $(\tilde{x}'_i, y_i) \in \tilde{D}_{ext}$ **do**
- 7: Fine-tuning the infected model $f(\tilde{x}'_i; \theta')$ according to Eq.(7)
- 8: Obtain purified model parameter θ^c
- 9: Stage-3 (optional): clean fine-tuning
- 10: **for** $(x_i, y_i) \in D_{ext}$ **do**
- 11: Further fine-tuning the purified model $f(x_i; \theta^c)$
- 12: **return** Advanced purified model parameter θ^{c+}

with \tilde{D}_{ext} , which produces purified model θ^c , *i.e.*,

$$\theta^c = \arg \min_{\theta} \mathbb{E}_{(\tilde{x}'_i, y_i) \in \tilde{D}_{ext}} [L(\tilde{x}'_i, y_i; \theta)] \quad (7)$$

s.t. $\theta_{init} = \theta'$

Since adversarial examples come from all image classes, they are associated with all possible class labels. According to the similarity between adversarial examples and triggered samples, when we fine-tune the infected model with adversarial examples, it mimics fine-tuning the model with triggered samples, yet the associated labels are not just the target-label but all possible class labels.

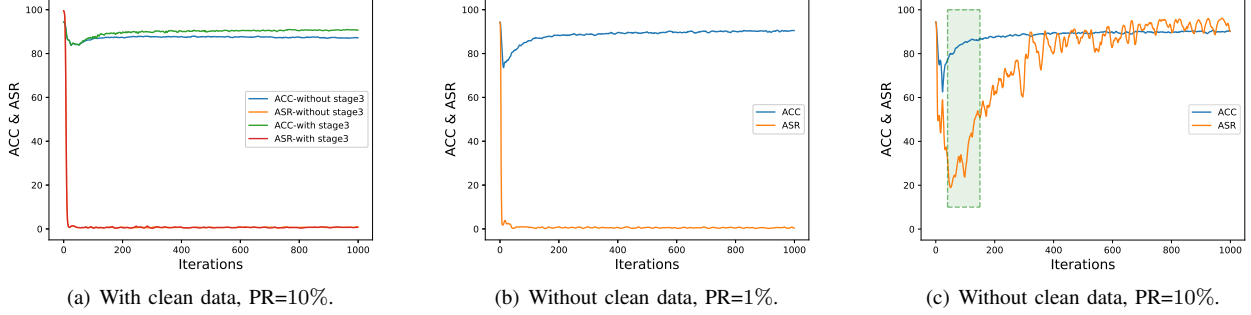


Fig. 3: The ASR and ACC vary with respect to the iterations of adversarial fine-tuning. PR is poisoning ratio.

Note that the foundation of backdoor attacks is to build a strong correlation between a trigger pattern and a target-label, which is achieved by poisoning training data, *i.e.*, to associate triggered samples with target-labels. As a result, our fine-tuning approach will break such a strong correlation and hence can achieve a defensive effect.

Without Clean Data: It is known that all previous defense methods require an additional clean dataset, but it is unavailable in some real applications. In this case, we find that our approach still has defensive effects when we could access the training data *even they are poisoned*. It significantly distinguishes our approach from the existing defense methods.

In particular, we only need to replace the additional clean images with those poisoned training images to generate adversarial examples. And then, we conduct adversarial fine-tuning on the infected model with those adversarial examples. Note that the 3rd-stage in Algorithm 1 is dropped in this case.

The experimental results show that we achieve a sufficient defensive effect when the poisoning ratio is less than 1%. The poisoning ratio is defined as the ratio of the poisoned samples to all training samples. 1% poisoning ratio is enough for most backdoor attacks, and is commonly adopted by most backdoor attacks in real-world applications [10].

We also test our approach for a high poisoning ratio (*e.g.*, 10% poisoning ratio). We evaluate how the attack success rate (ASR) varies with respect to the iterations of adversarial fine-tuning. As shown in Figure.3(c), at the beginning of the iterations, ASR drops quickly and significantly, and then it raises slowly. It is clear that ASR will go back high after excessive fine-tuning, which indicates performance degradation of our defense. However, by using an early stop scheme for the fine-tuning, we could obtain a model which has low ASR as well as high ACC, as illustrated by the green region in Figure.3(c). In other words, even for the case of a high poisoning ratio, we could conduct a few steps of adversarial fine-tuning to achieve a trade-off between ASR and ACC.

IV. EXPERIMENT

A. Experimental Setting

Backdoor Attacks and Configurations. We consider 5 state-of-the-art backdoor attacks: 1) BadNets [7], 2) Blend attack [23] 3) Sinusoidal signal attack(SIG) [9], 4) Input-aware

dynamic attack(DynamicAtt) [13], and 5) Warpping-based attack(WaNet) [8]. We test the performance of all attacks and erasing methods on two benchmark datasets, CIFAR-10 [43] and GTSRB [44]. For a fair evaluation, we use WideResNet (WRN-16-1*) [45] as the baseline model for the first three attacks, aligned with NAD [17], and for the latter two attacks, we use Pre-activation Resnet-18 [46] as the baseline model, aligned with the original paper [8], [13]. For the hyperparameters of adversarial perturbations, we adaptively set them to different values for each backdoor attack. More details on attack configurations are summarized in the supplemental material.

Backdoor Defense and Configuration. We compare our AFT approach with 4 existing backdoor erasing methods: 1) the standard Fine-tuning [14], 2) Fine-pruning [15], 3) the Neural Cleanse (NC) [24], and 4) Neural Attention Distillation (NAD) [17]. Regarding the additional clean data, we follow the same protocol of these methods: the additional clean data is randomly selected from clean training data, taking about 5% of all training data.

Evaluation Metrics. We evaluate the performance of defense mechanisms with two metrics: attack success rate (ASR), which is the ratio of triggered examples those are misclassified as the target label, and model’s accuracy on clean samples (ACC). An ideal defense should lead to large ASR drops with small ACC penalties.

B. More Results for Our Observation

1) Predicted Labels v.s. Target-labels.: Fig.1 has illustrated one example for our observation that the adversarial examples are highly likely classified as target-label, where 1) the dataset is CIFAR-10; 2) and the backdoor attack is WaNet which adopts warping as trigger embedding function. In this section, we illustrate that such observations are present regardless of which datasets are, what kinds of attacks are, and what trigger embedding functions are.

We verify our observations on both CIFAR-10 and GTSRB datasets, for both All-to-one and All-to-all backdoor attack settings, across all 5 backdoor attacks as well as different trigger embedding functions. We have the same observation, *i.e.*, the dominant predicted labels always align to the target-labels, as shown by the diagonal of the matrix in Fig.4.

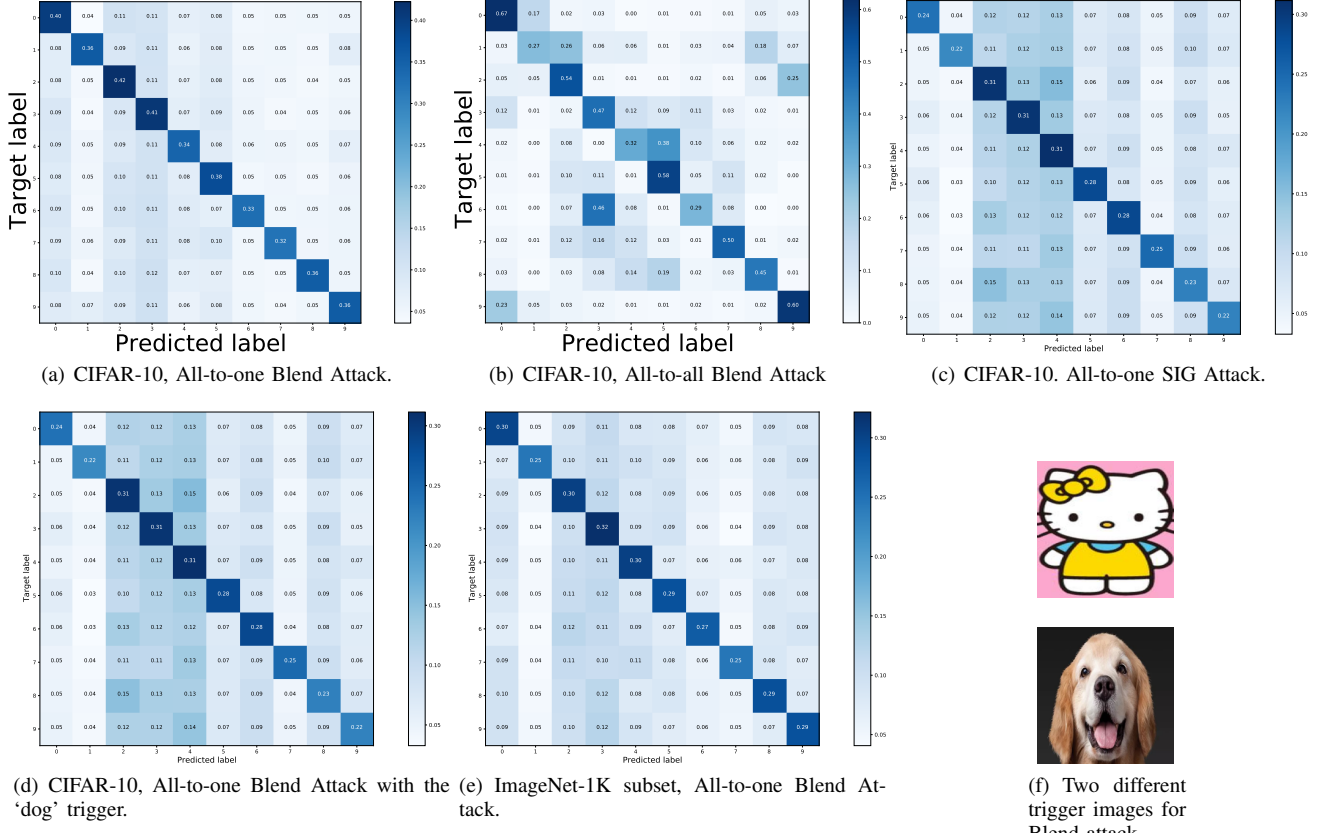


Fig. 4: Predicated labels v.s. Target-labels for randomly sampled adversarial examples \tilde{x}' , across different datasets and different backdoor attacks. No matter what kind of backdoor attack is (e.g., All-to-one or All-to-all), what attack is (e.g., WaNet or Blend), and what dataset is (e.g., CIFAR-10 or GTSRB), the dominate predicted labels always align to the target-labels, as shown by the diagonal of the matrix.

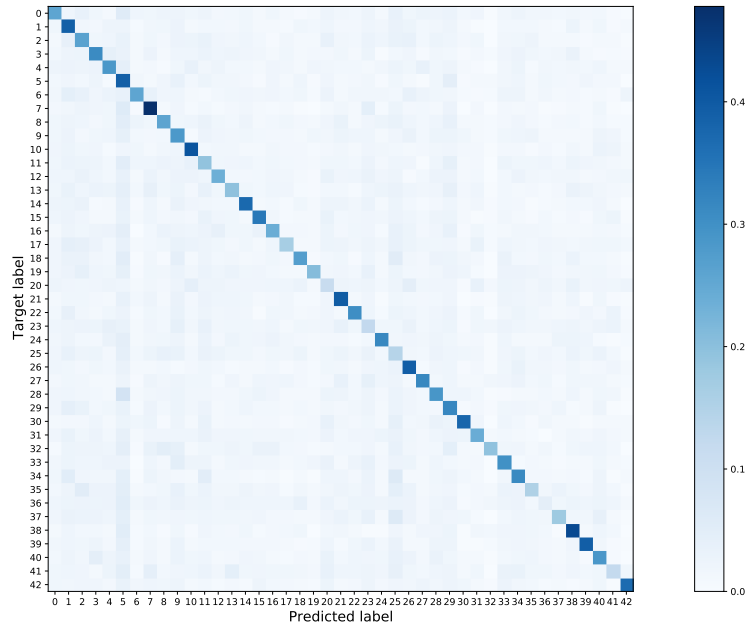


Fig. 5: Predicted labels v.s. Target-labels for WaNet attack on full GTSRB dataset.

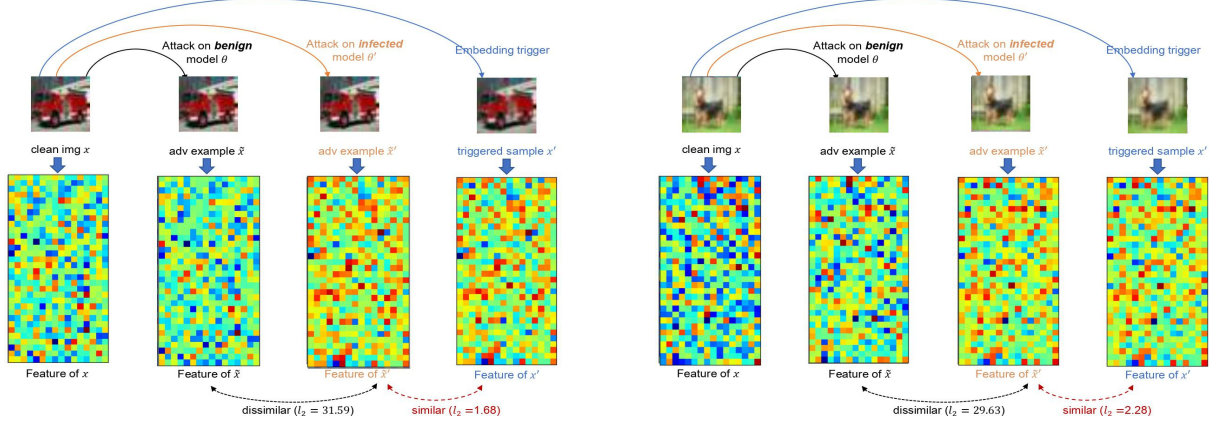


Fig. 6: The two images are sampled from CIFAR-10, with size of 32×32 , under WaNet Attack

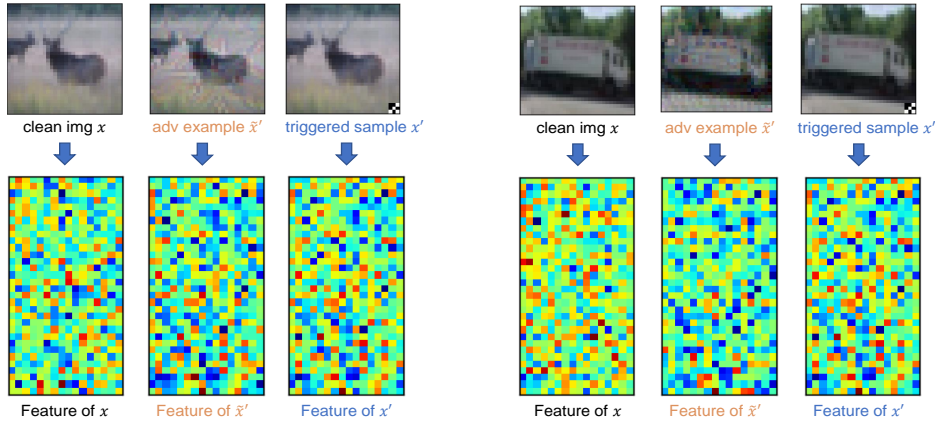


Fig. 7: The two images are sampled from CIFAR-10, with size of 32×32 , under BadNet Attack.

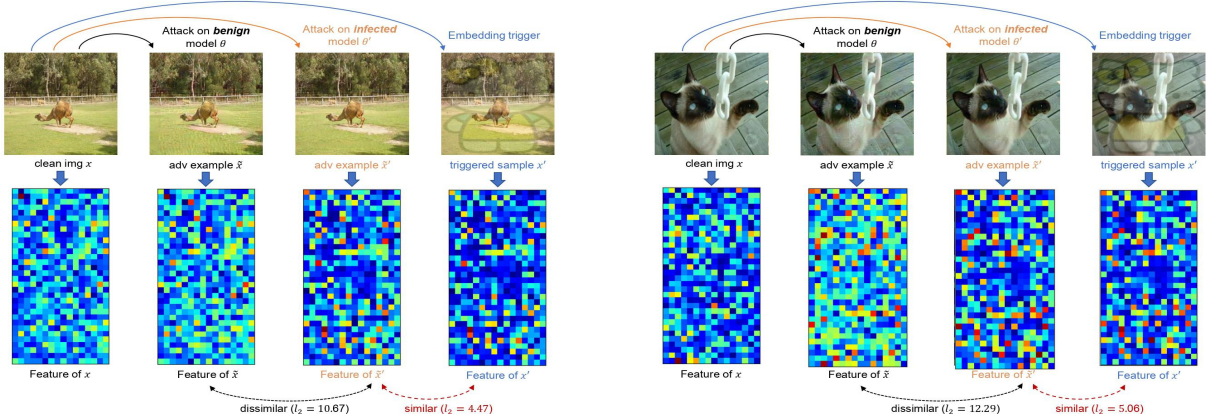


Fig. 8: Two images are sampled from ImageNet-1K, with size of 224×224 , under Blend Attack.

TABLE I: Quantitative comparisons for feature similarity.

	Badnet	SIG	Blend	DynamicAtt	WaNet
D_{benign}	102.58	135.91	124.22	40.42	48.13
D_{infected}	85.11	78.18	75.09	28.66	15.85

Fig.4(a), Fig.4(b) and Fig.4(c) are the results for All-to-one Blend backdoor attacks, All-to-all Blend backdoor attacks and All-to-one SIG backdoor attacks on CIFAR-10 dataset respectively. And The Fig.5 shows the full results for the WaNet attack on GTSRB dataset. These results indicate that our observation is a *general* observation.

Next we will give more results for different configurations to illustrate that our observations are present regardless of what dataset is, what backdoor attacks are, and what trigger embedding functions are.

Fig.4(d) are also the results for All-to-one Blend backdoor attacks on CIFAR-10 dataset. Regarding the Fig.4(d), we select the ‘dog’ image (ref to Fig.4(f)) as the trigger, rather than the ‘hello kitty’ image (ref to Fig.4(f)) used in the Fig.4(a). Compared to the Fig.4(a) in the above, it illustrates that we have the same observations regardless of what trigger images are chose. Regarding the Fig.4(e), we randomly select 10 out of 1000 classes from ImageNet-1K dataset, where the image sizes are 224×224 . It indicates that we have the same observations regardless of what image sizes are.

2) *Comparisons of Feature Similarity*.: Fig.2 gives one example to illustrate that the features of $\tilde{\mathbf{x}}'$ are very similar to that of triggered image \mathbf{x}^t , rather than $\tilde{\mathbf{x}}$. Here we give more results for the similarity of features among benign model’s adversarial examples $\tilde{\mathbf{x}}$, infected model’s adversarial examples $\tilde{\mathbf{x}}'$, and triggered samples \mathbf{x}^t . Figure.8 is an image from ImageNet-1K, which sizes are of 224×224 .

We also conduct more quantitative comparisons. We randomly sample 10,000 images from CIFAR-10, and calculate the l_2 distances between the features of $\tilde{\mathbf{x}}'$ and \mathbf{x}^t , i.e., $D_{\text{infected}} = \|\mathbf{f}(\tilde{\mathbf{x}}'), \mathbf{f}(\mathbf{x}^t)\|_2$. Meanwhile, we also calculate the l_2 distances between the features of $\tilde{\mathbf{x}}$ and \mathbf{x}^t , i.e., $\|D_{\text{benign}} = \mathbf{f}(\tilde{\mathbf{x}}), \mathbf{f}(\mathbf{x}^t)\|_2$. Regarding image features $\mathbf{f}()$, we adopt the output of the last convolution layer (just before the fully-connected layer) as image features. From Table I, we can see that after planting a backdoor into a model, the feature distances D_{infected} is smaller than D_{benign} significantly. Furthermore, we have **theoretically justified** our observations for the case of a linear model, which is shown in Sec V.

C. Comparison to Sota Defense Methods.

In order to illustrate the effectiveness of our proposed AFT defense, we evaluate its performance against 5 backdoor attacks using two metrics (i.e. ASR and ACC). Furthermore, we compare the performance of AFT with the other 4 existing backdoor defense methods.

Since all previous methods assume there is an additional clean dataset, we follow such protocol in this Section. The comparisons are shown in Table.II and Table.III.

From Table.II on the CIFAR-10 dataset, we can see that our AFT defense remarkably brings the average ASR from

nearly 100% down to **2.4%**. In comparison, Fine-tuning [14], Fine-pruning [15], and NAD [17] are only able to reduce the average ASR to 14.50%, 84.42%, and 4.88% respectively.

From Table.III on the GTSRB dataset, our AFT defense still significantly brings the average ASR from nearly 100% down to **1.18%**. In comparison, Fine-tuning [14], Fine-pruning [15], and NAD [17] reduce the average ASR to 11.77%, 86.50%, and 2.13% respectively.

Besides, it is obvious that NC [24] cannot defense against dynamic trigger attacks (*i.e.*, DynamicAtt, WaNet).

1) *Evaluation for All-to-all attack setting*.: The previous comparisons are evaluated under the All-to-one attack setting, and we further evaluate our approach under the All-to-all attack setting. Following previous methods [8], we set target-label as $y + 1$. From Table.IV, it is obvious that our approach is also very effective in this attack setting.

2) *Evaluation on Large-scale Dataset*.: To further evaluate our approach on the large-scale dataset, we conduct defense experiments on the Tiny-ImageNet dataset [47]. The original Tiny-ImageNet contains 100,000 images of 200 classes down-sized to 64×64 colored images. In order to reload the pre-trained weights associated to the standard ImageNet dataset, the images are usually resized back to 224×224 in previous methods [48].

We also follow the same protocol to use 224×224 image resolution, and adopt Resnet-18 as the baseline classification model. The other experimental setting is the same as that for CIFAR-10 and GTSRB. From Table.V, We can see that our approach is effective on large-scale Dataset.

D. Without Additional Clean Data.

When an additional clean dataset is unavailable, all existing defense methods cannot work. But our approach still has some defensive effects if we could access the training data *even though they are poisoned*. In particular, we only need to replace the additional clean images with those poisoned training images to generate adversarial examples. And then, those generated adversarial examples are used to purify the infected model. Note that the 3rd-stage is dropped in this case.

We find that our defensive effect depends on the poisoning ratio. Normally, the defensive effect improves with the decrease of the poisoning ratio. As shown in Fig.9, Blend attack could achieve a strong attack effect ASR=90.36% at PR=1% on CIFAR-10 data. But our AFT defense could bring the ASR down to 1.76% at PR=1%.

Small Poisoning Ratio. Generally, a 1% poisoning ratio is enough and commonly adopted by most backdoor attacks in real-world applications. So, we evaluate our AFT defense with PR=1%. As shown in Table.VI, our AFT defense still brings the average ASR from nearly 100% down to **4.13%** on the CIFAR-10 dataset. From Table.VII, we also see that our AFT defense could reduce ASR to **3.68%** on GTSRB dataset.

As we know, all other backdoor defense methods cannot work without clean data. Thus, the performance of Fine-tuning, Fine-pruning and NAD in Table.VI and Table.VII is evaluated under the condition that the clean data is **used**. Comparing the NAD in Table.VI and Table.II (PR=10% vs. PR=1%, both use

TABLE II: Comparison with SoTA defense methods against the **All-to-one** backdoor attack on **CIFAR10**, where the additional clean dataset is **used by all defense methods**. The poisoning ratio is set as PR=10%. Our AFT defense remarkably brings the average ASR from nearly 100% down to 2.4%. In comparison, Fine-tuning, Fine-pruning, and NAD are only able to reduce the average ASR to 16.9%, 92.6%, and 4.85% respectively.

	Before		Fine-tuning [14]		Fine-pruning [15]		Neural Cleanse [24]		NAD [17]		AFT (Ours)	
	ACC	ASR	ACC↑	ASR↓	ACC↑	ASR↓	ACC↑	ASR↓	ACC↑	ASR↓	ACC↑	ASR↓
Badnet	85.55	100.00	81.13	14.17	80.32	80.37	82.22	2.43	81.30	4.36	81.79	2.37
Blend	85.07	99.04	81.03	26.54	80.97	71.31	82.32	2.63	82.90	4.84	81.68	3.88
SIG	84.02	98.78	80.98	10.21	80.33	72.10	81.78	2.79	82.00	2.25	82.34	2.67
DynamicAtt	94.65	99.24	94.00	8.77	89.91	98.97	94.65	99.24	94.23	4.59	93.25	1.62
WaNet	94.15	99.50	93.42	12.80	89.86	99.36	94.15	99.50	94.02	8.37	94.06	1.46

TABLE III: Comparison with SoTA defense methods against the **All-to-one** backdoor attack on **GTSRB**, where the additional clean dataset is **used by all defense methods**. The poisoning ratio is set as PR=10%. Our AFT defense remarkably brings the average ASR from nearly 100% down to 1.18%, while NAD only reduce the average ASR to 2.13%.

	Before		Fine-tuning [14]		Fine-pruning [15]		Neural Cleanse [24]		NAD [17]		AFT (Ours)	
	ACC	ASR	ACC↑	ASR↓	ACC↑	ASR↓	ACC↑	ASR↓	ACC↑	ASR↓	ACC↑	ASR↓
Badnet	97.68	100.00	93.39	14.20	92.30	79.20	94.15	0.08	92.22	0.33	92.79	0.12
Blend	97.16	99.21	93.02	20.31	92.95	87.81	93.79	1.67	93.08	3.43	92.91	2.23
SIG	97.39	99.96	93.34	3.83	92.68	69.42	94.03	0.24	92.98	0.88	93.15	0.13
DynamicAtt	99.27	99.84	99.10	16.33	89.15	97.21	99.27	99.84	99.17	3.80	96.68	2.99
WaNet	98.97	98.78	98.70	4.20	87.49	98.79	98.87	98.78	98.87	2.20	98.58	0.47

TABLE IV: Comparison with SoTA defense methods against the **All-to-all** backdoor attack on **CIFAR10**, where the additional clean dataset is **used by all defense methods**. The poisoning ratio is set as PR=10%. Our AFT defense remarkably brings the average ASR from nearly 85.38% down to 2.1%. In comparison, Fine-tuning, and NAD are only able to reduce the average ASR to 5.26%, and 3.22% respectively.

	Before		Fine-tuning [14]		NAD [17]		AFT (Ours)	
	ACC	ASR	ACC↑	ASR↓	ACC↑	ASR↓	ACC↑	ASR↓
Badnet	85.45	82.81	80.54	3.36	81.07	3.12	82.06	2.67
Blend	84.53	80.87	80.48	5.32	81.85	3.67	82.75	2.26
SIG	82.94	76.99	76.27	5.34	80.55	4.23	79.59	4.35
DynamicAtt	94.40	92.72	92.05	4.46	92.71	1.39	93.28	0.75
WaNet	94.49	93.47	93.37	7.81	93.68	3.69	93.08	0.80

TABLE V: Evaluation on Tiny-ImageNet

ACC/ASR	Badnet		SIG		Blend	
Before	68.45	99.89	68.12	99.74	67.83	97.30
AFT	63.23	1.65	62.58	1.19	62.37	4.19

clean data), take the same attack Blend as an example we see that NAD defense could further reduce ASR from 4.88% to 2.59%. It indicates that the defense effect of NAD improves with the decreasing of poisoning ratio, which aligns with Fig.9.

More importantly, Table.VI and Table.VII tell us that our AFT defense can outperform or be comparable to the other 3 defense methods even we do not use the clean data. For instance, our AFT outperforms NAD against Blend attack, while it is a little worse than NAD against SIG attack.

Large Poisoning Ratio. We also evaluate our approach for a large poisoning ratio, *e.g.*, PR=10%. As aforementioned in Fig.3(c), since the ASR first drops quickly and then raises

slowly, we could obtain low ASR as well as high ACC by adopting an early stop scheme. From Table.VIII, we see that our AFT defense could still bring the average ASR down to **20.2%** while remaining ACC at **70%** on CIFAR-10.

Besides, comparing the AFT in Table.VIII and Table.II (without vs. with clean data, both have PR=10%), take the same attack Badnet as an example we see that the defensive effect of our AFT become worse if the additional clean data is not used, *i.e.*, the ASR degrades from 2.37% to 14.11%.

E. Comprehensive Analysis of AFT

1) *Without 3rd-Stage in Algorithm 1.:* Algorithm 1 in our approach includes three stages, where the backdoor is assumed to be erased after the second stage and the third stage aims to further improve the ACC of the purified model.

In this section, we will show that the 3rd-stage could be used to make a trade-off between the ACC and ASR. From Fig.3(a), we can see that if the third stage is included there is an obvious improvement on ACC at the cost of marginal

TABLE VI: Comparison with SoTA defense methods on **CIFAR10**. Note that the additional clean data is only used by Fine-tuning, Fine-pruning, and NAD. But our AFT **does not use the additional clean data**. The poisoning ratio is set as PR=1%. Our AFT can outperform or comparable to the other 3 defense methods even we do not leverage the clean data.

	Before		Fine-tuning [14]		Fine-pruning [15]		NAD [17]		AFT (Ours)	
	ACC	ASR	ACC↑	ASR↓	ACC↑	ASR↓	ACC↑	ASR↓	ACC↑	ASR↓
Badnet	84.31	97.97	81.38	16.44	81.44	71.08	80.87	2.84	79.47	4.92
Blend	82.96	87.53	80.44	8.50	80.03	68.01	80.88	2.93	79.80	2.52
SIG	81.83	95.02	79.22	6.31	80.11	65.78	80.10	1.96	78.38	4.97

TABLE VII: Comparison with SoTA defense methods on **GTSRB**. Note that the additional clean data is only used by Fine-tuning, Fine-pruning, and NAD. But our AFT **does not use the additional clean data**. The poisoning ratio is set as PR=1%.

	Before		Fine-tuning [14]		Fine-pruning [15]		NAD [17]		AFT (Ours)	
	ACC	ASR	ACC↑	ASR↓	ACC↑	ASR↓	ACC↑	ASR↓	ACC↑	ASR↓
Badnet	98.22	99.94	91.82	10.80	92.67	60.53	93.00	0.76	91.33	2.25
Blend	98.02	92.84	92.88	21.10	92.08	79.94	93.02	2.72	91.29	1.92
SIG	97.37	98.96	92.98	6.88	93.01	67.30	93.17	2.79	87.39	6.87

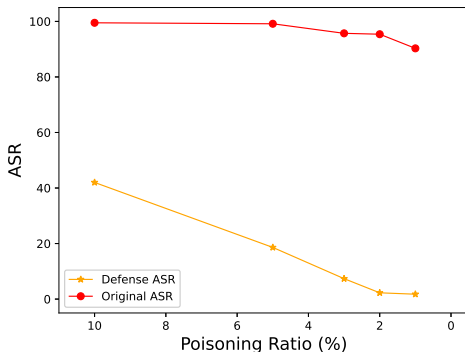


Fig. 9: ASR v.s. Poisoning Ratio. Defensive effect improves with the decrease of poisoning ratio.

TABLE VIII: Our AFT defense for large poisoning ratio (**PR=10%**) on CIFAR-10 **without** an additional clean data. The defensive effect become worse if the additional clean data is not used.

	ACC↑	ASR↓
Badnet	70.02	14.11
Blend	70.28	18.06
SIG	70.04	28.50

ASR degradation. More quantitative comparisons are shown in Table. IX, the 3rd-stage could boost average ACC from 83.89% to 86.7%, while the average ASR degrade from 2.11% to 2.4%.

Note that if the adversarial perturbation used in the first stage is strong, there will be a moderate drop of ACC after

TABLE IX: Ablation study of 3rd-stage in Algorithm 1.

	w/o 3rd-stage		w/ 3rd-stage	
	ACC↑	ASR↓	ACC↑	ASR↓
Badnet	78.08	2.56	81.79	2.37
Blend	78.76	2.89	81.68	3.88
SIG	76.04	2.58	82.34	2.67
DynamicAtt	92.54	1.81	93.65	1.62
WaNet	94.03	0.75	94.06	1.46

TABLE X: Ablation of Data Augmentation.

	w/o data-aug		w/ data-aug	
	ACC↑	ASR↓	ACC↑	ASR↓
	73.08	12.08	79.47	4.92

the first stage. Thus, it will be necessary to conduct the 3rd-stage to get the ACC improved back.

2) *Data Augmentation*.: We have discussed that our approach could have a certain defensive effect when we have no additional clean data, even with a large poisoning ratio (refer to Sec.IV-D). In this experiment, we will illustrate that data augmentation is a very helpful trick for this situation.

Since the additional clean data is replaced with poisoned training data as generating adversarial examples, we hope to reduce the effect of triggers in the poisoned data so as to purify the poisoned data.

On the other hand, some trigger embedding schemes in backdoor attacks are often defined with a specific spatial position. For instance, patch-based backdoor attacks often determine a specific image region to add the trigger patch. Therefore, we could purify poisoned data by using the data

augmentation trick. It is due to that data augmentation could disturb the spatial pattern in the trigger embedding. Obviously, data augmentation should be very effective to those location-sensitive backdoor attacks such as patch-based attacks (e.g., BadNets [7]).

Specifically, we conduct random cropping and flipping for images in D'_{train} (refer to Eq.(6)), which produces augmented dataset D'_{train+} . And then we generate adversarial examples on D'_{train+} .

We compare the defensive performance of our AFT against BadNets with and without this data augmentation. From Table, we see that on the CIFAR-10 dataset this trick could significantly boost the ASR from 12.08% to 4.92%.

V. THEORETICAL ANALYSIS

In previous sections, we have empirically shown the observations that for an infected model, the features of adversarial examples \tilde{x}' are very similar to the features of triggered images x^t , which results in that \tilde{x}' is highly likely classified as the target-label l instead of any other classes. In this section, we take a linear classification model as an example to theoretically justify that our observation does make sense.

A. Structure of Infected Model W^*

Let $(x_i, y_i), i = 1, \dots, n$ be the training examples, where $x_i \in \mathbb{R}^d$ and $y_i \in [K]$. Let $n_j, j \in [K]$ be the number of instances in class C_j . All the training examples are well normalized, i.e. $|x_i| = 1, i \in [n]$. We assume all the training instance x_i living a subspace $\mathcal{S}_m \subset \mathbb{R}^d$ of m dimension, with $m < d$. For the simplicity of our analysis, we assume the trigger embedding function $Trigger()$ is to add a pre-defined patch P to an input image, i.e.,

$$x^t = Trigger(x) = x + P \quad (8)$$

Since the image patch $P \in \mathbb{R}^d$ introduced is very different from most training examples $\{x_i\}_{i=1}^n$, it is safe to assume that P is orthogonal to \mathcal{S}_m . In the backdoor attack, we randomly sample ℓ examples from class C_l , and embed the trigger P into them. Thus, the infected linear classifiers, denoted by $W = (w_1, w_2, \dots, w_K)$, are obtained by solving the following optimization problem

$$W^* = \arg \min_{W \in \mathbb{R}^{d \times K}} \mathcal{F}(W) \quad (9)$$

where

$$\mathcal{F}(W) = -\frac{1}{n} \sum_{i=1}^n \log \frac{\exp(\langle w_{y_i}, x_i \rangle)}{\sum_{j=1}^K \exp(\langle w_j, x_i \rangle)} + \frac{\lambda}{2} |W|_F^2 \quad (10)$$

Define \tilde{W}^* be the solution, with each column vector restricted to the subspace \mathcal{S}_m , that minimizes $\mathcal{F}(W)$, i.e.

$$\tilde{W}^* = \arg \min_{\tilde{W} \in \mathcal{A}} \mathcal{F}(\tilde{W}) \quad (11)$$

where

$$\mathcal{A} = \left\{ \tilde{W} \in \mathbb{R}^{d \times K} : W_{*,j} \in \mathcal{S}_m, j \in [K] \right\}$$

Obviously, \tilde{W}^* can be regarded as the benign model, which is trained with clean images instead of triggered images. The

following lemma characterizes the structure of the optimal solution W^* obtained from (9).

Lemma 1: Rewrite $W^* = W_{\parallel}^* + W_{\perp}^*$, where W_{\parallel}^* is the projection of column vectors in W^* into the subspace \mathcal{S}_m . We have

$$|W_{\parallel}^* - \tilde{W}^*| \leq \frac{\ell|P|^2}{\sqrt{2}\lambda}$$

and $W_{\perp}^* = Pu^{\top}$, where $u \in \mathbb{R}^d$, with $u_j \leq 0$ for $j \neq l$ and

$$u_l \geq \frac{(\sqrt{2}-1)\ell|P|^2}{\sqrt{2}\lambda}$$

Proof: Due to the presence of regularizer $\lambda|W|_F^2/2$, it is easy to see that the optimal solution W^* can be written as $W^* = W_{\parallel}^* + Pu^{\top}$, with W_{\parallel}^* being the projection of W^* into the subspace \mathcal{S}_m . It is also easy to show that $u_l \geq 0$ and $u_j \leq 0, j \neq l$ by simply checking out the derivative of the objective function with respect to u_j and u_l .

We construct the upper bound for $\mathcal{F}(W^*)$. To this end, we restrict the solution to the form of $\tilde{W} + \gamma P\mathbf{e}_l$, where \mathbf{e}_l is a binary vector with all its elements being zero except for the l -th element. The resulting optimization problem is given by

$$\min_{\tilde{W} \in \mathcal{A}, \gamma \geq 0} -\ell|P|^2\gamma + \frac{\lambda}{2}\gamma^2 + \mathcal{F}(\tilde{W})$$

The resulting solution is $W_1 = \tilde{W}^* + \gamma P\mathbf{e}_l$, with $\gamma = \ell|P|^2/\lambda$, and optimal value is $\mathcal{F}(W_1) = \mathcal{F}(\tilde{W}^*) - \ell^2|P|^4/[2\lambda]$. Evidently, we have

$$\mathcal{F}(W^*) \leq \mathcal{F}(\tilde{W}^*) - \frac{\ell^2|P|^4}{2\lambda} \quad (12)$$

We then proceed to construct the lower bound for $\mathcal{F}(W^*)$. Define $u' = \max\{|u_j| : j \neq l\}$. Since for each training x_i in the class C_l that is triggered with P , its negative log-likelihood is bounded as

$$\begin{aligned} & -\log \frac{\exp(\langle w_l, x_i \rangle)}{\sum_{j=1}^K \exp(\langle w_j, x_i \rangle)} \\ & \geq -(u_l + u')|P|^2 - \log \frac{\exp(\langle \tilde{w}_l, x_i \rangle)}{\sum_{j=1}^K \exp(\langle \tilde{w}_j, x_i \rangle)} \end{aligned}$$

where $\tilde{w}_j \in \mathcal{S}_m, j \in [K]$. As a result, we have the following lower bound for $\mathcal{F}(\tilde{W}^*)$, i.e.

$$\min_{\tilde{W} \in \mathcal{A}, u_l, u' \geq 0} -\ell|P|^2(u_l + u') + \frac{\lambda}{2}(|u_l|^2 + |u'|^2) + \mathcal{F}(\tilde{W})$$

which can be further simplified as

$$\min_{\tilde{W} \in \mathcal{A}, \gamma \geq 0} -\ell|P|^2\gamma + \frac{\lambda}{4}\gamma^2 + \mathcal{F}(\tilde{W})$$

By solving the above optimization problem, we have $\mathcal{F}(W^*)$ lower bounded as

$$\mathcal{F}(W^*) \geq \mathcal{F}(\tilde{W}^*) - \frac{\ell^2|P|^4}{\lambda} \quad (13)$$

Using the upper and lower bounds from (12) and (13), we have

$$\mathcal{F}(W_1) - \mathcal{F}(W^*) \leq \frac{\ell^2|P|^4}{2\lambda}$$

Since $\mathcal{F}(W)$ is λ -strong convex, we have

$$|W_1 - W_*|^2 \leq \frac{\ell^2 |P|^4}{2\lambda^2}$$

The lemma will then directly follows from the above inequality. \blacksquare

The above lemma tells us that **for the infected model W^* , its component W_{\parallel}^* is not too far from the benign model \widetilde{W}^* , while the residual component W_{\perp}^* will give a strong response to the trigger P .** It means that planting a backdoor into a model will not strongly affect the model's performance on benign images, but **will significantly affect its predictions on triggered images**.

In addition, this lemma tell us the interesting role played by ℓ , the number of instances sampled from class C_l to be triggered by P : a larger ℓ will lead to a larger value of u_l , indicating a stronger footprint of pattern P implemented in the l th classifier; but, at the same time, a larger ℓ will lead to a larger value $|W_{\parallel}^* - \widetilde{W}^*|$, implying a distortion in classification models. Hence, an appropriate choice of ℓ should result in a small distortion in the overall classification model, and at the same time, a strong enough backdoor attack of trigger P in the classification model for class C_l .

B. Structure of Perturbation \mathbf{r}

After analyzing the structure of the solution learned from triggered examples, we proceed to analyze the perturbation \mathbf{r} learned from adversarial attack by solving the following optimization problem

$$\mathbf{r} = \max_{|\mathbf{r}| \leq \delta} \mathcal{L}(\mathbf{r}) \quad (14)$$

where

$$\mathcal{L}(\mathbf{r}) = \frac{1}{\sum_{i=1}^n [y_i \neq l]} \sum_{i:y_i \neq l} \min_{j \neq k} f_k(x_i + \mathbf{r}) - f_j(x_i + \mathbf{r}) \quad (15)$$

In the above, we introduce $\delta \ll 1$ to specify the magnitude of perturbation, and $f_j(\cdot)$ for the classification model for the j -th class. The underlying logic is to find a small perturbation \mathbf{r} that will make the deep model predict class C_l for every instance.

To simplify our analysis, we assume that the original training examples (without any trigger) can be perfectly classified with margin $\tau > 0$, i.e.

$$\tau = \min_{i \in [n]} \min_{j \neq y_i} \langle \tilde{w}_{y_i}^* - \tilde{w}_j^*, x_i \rangle$$

We assume that τ is large enough such that a small perturbation made to \widetilde{W}^* will not affect classification result, i.e.

$$\tau \geq \frac{\sqrt{2}\ell|P|^2}{\lambda} \quad (16)$$

We finally assume δ is small enough, i.e.

$$\delta \leq \frac{\tau/2}{\min_{j \neq l} |\tilde{w}_l^* - \tilde{w}_j^*| + \ell|P|^2/[\sqrt{2}\lambda]} \quad (17)$$

Theorem 1: Under the assumptions in (17) and (16), we have \mathbf{r}_{\perp} , the projection of \mathbf{r} on the direction of P , bounded as

$$v \frac{|\mathbf{r}_{\perp}|}{|\mathbf{r}|} \geq \frac{(\sqrt{2}-1)\ell|P|^2}{\sqrt{(\sqrt{2}-1)^2\ell^2|P|^4 + (\ell|P|^2 + \sqrt{2}K/(\exp(\tau) + K))^2}}$$

Proof: Now, we consider the adversarial training by maximizing $\mathcal{L}(\mathbf{r})$, which is given as

$$\mathcal{L}(\mathbf{r}) = \frac{1}{\sum_{i=1}^n [y_i \neq l]} \sum_{i:y_i \neq l} \min_{j \neq l} \langle w_l^* - w_j^*, x_i + \mathbf{r} \rangle$$

Under the assumptions in (16) and (17), we can rewrite $\mathcal{L}(\mathbf{r})$ as

$$\mathcal{L}(\mathbf{r}) = \frac{1}{\sum_{i=1}^n [y_i \neq l]} \sum_{i:y_i \neq l} \langle w_l^* - w_{y_i}^*, x_i + \mathbf{r} \rangle \quad (18)$$

This is because, according to the definition of classification margin τ , we have, for any instance x_i with $y_i \neq l$,

$$\langle \tilde{w}_{y_i}^* - \tilde{w}_j^*, x_i \rangle \geq \tau, \forall j \neq y_i$$

Since

$$|w_{\parallel,y_i}^* - w_{\parallel,j}^* - (\tilde{w}_{y_i}^* - \tilde{w}_j^*)| \leq |W_{\parallel}^* - \widetilde{W}^*| \leq \frac{\ell|P|^2}{\sqrt{2}\lambda}$$

using the condition in (16), we have, for any instance x_i with $y_i \neq l$,

$$\langle w_{\parallel,y_i}^* - w_{\parallel,j}^*, x_i \rangle \geq \frac{\tau}{2}, \forall j \neq y_i$$

Since $w_j^* = w_{\parallel,j}^* + u_j P$ and $P \perp x_i$ for any $y_i \neq l$, we have, for any x_i with $y_i \neq l$

$$\langle w_{y_i}^* - w_j^*, x_i \rangle \geq \frac{\tau}{2}, \forall j \neq l$$

Since

$$|w_{y_i}^* - w_j^*| \leq |\tilde{w}_{y_i}^* - \tilde{w}_j^*| + \frac{\ell|P|^2}{\sqrt{2}\lambda}, \forall j \neq y_i$$

using the condition in (17), we have

$$\langle w_{y_i}^* - w_j^*, \mathbf{r} \rangle \geq - \left(|\tilde{w}_{y_i}^* - \tilde{w}_j^*| + \frac{\ell|P|^2}{\sqrt{2}\lambda} \right) \delta \geq -\frac{\tau}{2}, \forall j \neq y_i$$

As a result, for any x_i with $y_i \neq l$, we have

$$\langle w_{y_i}^*, x + \mathbf{r} \rangle \geq \langle w_j^*, x + \mathbf{r} \rangle, \forall j \neq y_i$$

and therefore

$$\min_{j \neq l} \langle w_l^* - w_j^*, x_i + \mathbf{r} \rangle = \langle w_l^* - w_{y_i}^*, x_i + \mathbf{r} \rangle$$

which leads to the expression in (18). We then proceed to simplify the expression in (18)

$$\begin{aligned} \mathcal{L}(\mathbf{r}) &= \frac{1}{\sum_{i=1}^n [y_i \neq l]} \sum_{i:y_i \neq l} \langle w_l^* - w_{y_i}^*, x_i + \mathbf{r} \rangle \\ &= \frac{1}{\sum_{i=1}^n [y_i \neq l]} \sum_{i:y_i \neq l} \langle w_{\parallel,l}^* - w_{\parallel,y_i}^* + (u_l - u_{y_i})P, \\ &\quad x_i + \mathbf{r} \rangle \\ &= \frac{\langle P, \mathbf{r} \rangle}{\sum_{i=1}^n [y_i \neq l]} \sum_{i:y_i \neq l} (u_l - u_{y_i}) \\ &\quad + \frac{1}{\sum_{i=1}^n [y_i \neq l]} \sum_{i:y_i \neq l} \langle w_{\parallel,l}^* - w_{\parallel,y_i}^*, x_i + \mathbf{r} \rangle \end{aligned}$$

Write $\mathbf{r} = \mathbf{r}_\perp + \mathbf{r}_\parallel$, where \mathbf{r}_\parallel is the projection of \mathbf{r} into the subspace \mathcal{S}_m . Using these notation, we have

$$\begin{aligned}\mathcal{L}(\mathbf{r}) &= \frac{\langle P, \mathbf{r}_\perp \rangle}{\sum_{i=1}^n [y_i \neq l]} \sum_{i:y_i \neq l} (u_l - u_{y_i}) \\ &\quad + \frac{1}{\sum_{i=1}^n [y_i \neq l]} \sum_{i:y_i \neq l} \langle w_{\parallel, l}^* - w_{\parallel, y_i}^*, x_i + \mathbf{r}_\parallel \rangle\end{aligned}$$

Define

$$\begin{aligned}\alpha &= \frac{1}{\sum_{i=1}^n [y_i \neq l]} \sum_{i:y_i \neq l} (u_l - u_{y_i}), \\ v &= \frac{1}{\sum_{i=1}^n [y_i \neq l]} \sum_{i:y_i \neq l} w_{\parallel, l}^* - w_{\parallel, y_i}^*\end{aligned}$$

We have

$$|\mathbf{r}_\perp| = \frac{\alpha|P|\delta}{\sqrt{\alpha^2|P|^2 + |v|^2}} \quad (19)$$

Since $u_l \geq (\sqrt{2}-1)\ell|P|^2/[\sqrt{2}\lambda]$ and $u_j \leq 0$ for $j \neq l$, we have

$$\alpha \geq \frac{(\sqrt{2}-1)\ell|P|^2}{\sqrt{2}\lambda} \quad (20)$$

To bound $|v|$, we use the first order condition for the optimal solution \tilde{W}^* , i.e.

$$\tilde{w}_j^* = \frac{1}{\lambda} \sum_{i=1}^n \left([y_i = j] \left(1 - p(y_i|x_i; \tilde{W}^*) \right) - [y_i \neq j] p(j|x_i; \tilde{W}^*) \right) \quad [1]$$

where

$$p(j|x_i; \tilde{W}^*) = \frac{\exp(\langle \tilde{w}_j^*, x_i \rangle)}{\sum_{j'=1}^K \exp(\langle \tilde{w}_{j'}^*, x_i \rangle)} \quad [2]$$

Using the definition of classification margin, we have

$$1 - p(y_i|x_i; \tilde{W}^*) \leq \frac{K}{\exp(\tau) + K} \quad [3]$$

and

$$p(j|x_i; \tilde{W}^*) \leq \frac{1}{\exp(\tau) + K} \quad [4]$$

As a result, we have

$$|\tilde{w}_j^*| \leq \frac{K}{\lambda(\exp(\tau) + K)} \quad [5]$$

and

$$|w_{\parallel, l}^* - w_{\parallel, j}^*| \leq |\tilde{w}_l^* - \tilde{w}_j^*| + \frac{\ell|P|^2}{\sqrt{2}\lambda} \leq \frac{1}{\lambda} \left(\frac{\ell|P|^2}{\sqrt{2}} + \frac{K}{\exp(\tau) + K} \right) \quad [6]$$

We complete the proof by plugging the bounds from (20) and (21) into the expression (19). \blacksquare

From the above theorem, we can see that **when projecting perturbation r on the direction of trigger P , the projection \mathbf{r}_\perp take an significant part in the full perturbation r** . It means that the perturbation r is very similar to the trigger P , which **justify our observations that the adversarial examples $\tilde{x}' = x + r$ are similar to triggered images $x^t = x + P$** .

VI. CONCLUSION

In this work, we propose a new Adversarial Fine-Tuning approach to erase backdoor triggers by leveraging adversarial examples of the infected model. We find that both adversarial examples and triggered samples tend to be classified as target-labels, and their features are very similar to each other, which indicates that they will activate the same subset of DNN neurons. Such observations tell us that planting a backdoor into a model will significantly affect the model's adversarial examples. Generally, it implies an intrinsic connection between backdoor attacks and adversarial attacks. Unlike previous methods treating them as two distinct problems, we think building a connection between them would benefit the study for both of them.

In addition, based on such observations we propose a simple but effective defense method, *i.e.*, Adversarial Fine-Tuning, which can defend against 5 state-of-the-art backdoor attacks. Besides, our AFT approach outperforms state-of-the-art backdoor defense methods significantly. Even for the situation that the additional clean data is unavailable, our AFT could still achieve a sufficient defensive effect.

REFERENCES

- [1] I. J. Goodfellow, J. Shlens, and C. Szegedy, “Explaining and harnessing adversarial examples,” *arXiv preprint arXiv:1412.6572*, 2014.
- [2] C. Szegedy, W. Zaremba, I. Sutskever, J. Bruna, D. Erhan, I. Goodfellow, and R. Fergus, “Intriguing properties of neural networks,” in *2nd International Conference on Learning Representations, ICLR 2014*, 2014.
- [3] Y. Li, B. Wu, Y. Jiang, Z. Li, and S.-T. Xia, “Backdoor learning: A survey,” *arXiv preprint arXiv:2007.08745*, 2020.
- [4] A. Vaswani, N. Shazeer, N. Parmar, J. Uszkoreit, L. Jones, A. N. Gomez, L. Kaiser, and I. Polosukhin, “Attention is all you need,” in *NIPS*, 2017, pp. 5998–6008.
- [5] J. Devlin, M.-W. Chang, K. Lee, and K. Toutanova, “Bert: Pre-training of deep bidirectional transformers for language understanding,” *arXiv preprint arXiv:1810.04805*, 2018.
- [6] A. Dosovitskiy, L. Beyer, A. Kolesnikov, D. Weissenborn, X. Zhai, T. Unterthiner, M. Dehghani, M. Minderer, G. Heigold, S. Gelly *et al.*, “An image is worth 16x16 words: Transformers for image recognition at scale,” *arXiv preprint arXiv:2010.11929*, 2020.
- [7] T. Gu, B. Dolan-Gavitt, and S. Garg, “Badnets: Identifying vulnerabilities in the machine learning model supply chain,” *arXiv preprint arXiv:1708.06733*, 2017.
- [8] T. A. Nguyen and A. T. Tran, “Wanet-imperceptible warping-based backdoor attack,” in *International Conference on Learning Representations*, 2020.
- [9] M. Barni, K. Kallas, and B. Tondi, “A new backdoor attack in cnns by training set corruption without label poisoning,” in *2019 IEEE International Conference on Image Processing (ICIP)*. IEEE, 2019, pp. 101–105.
- [10] Y. Liu, X. Ma, J. Bailey, and F. Lu, “Reflection backdoor: A natural backdoor attack on deep neural networks,” in *European Conference on Computer Vision*. Springer, 2020, pp. 182–199.
- [11] A. Turner, D. Tsipras, and A. Madry, “Clean-label backdoor attacks,” 2018.
- [12] A. Shafahi, W. R. Huang, M. Najibi, O. Suciu, C. Studer, T. Dumitras, and T. Goldstein, “Poison frogs! targeted clean-label poisoning attacks on neural networks,” *Advances in neural information processing systems*, vol. 31, 2018.

[13] T. A. Nguyen and A. Tran, "Input-aware dynamic backdoor attack," *Advances in Neural Information Processing Systems*, vol. 33, pp. 3454–3464, 2020.

[14] Y. Liu, Y. Xie, and S. Ankur, "Neural trojans," in *International Conference on Computer Design (ICCD)*, 2017.

[15] K. Liu, B. Dolan-Gavitt, and S. Garg, "Fine-pruning: Defending against backdooring attacks on deep neural networks," in *International Symposium on Research in Attacks, Intrusions, and Defenses*. Springer, 2018, pp. 273–294.

[16] P. Zhao, P.-Y. Chen, P. Das, K. N. Ramamurthy, and X. Lin, "Bridging mode connectivity in loss landscapes and adversarial robustness," in *International Conference on Learning Representations*, 2019.

[17] Y. Li, X. Lyu, N. Koren, L. Lyu, B. Li, and X. Ma, "Neural attention distillation: Erasing backdoor triggers from deep neural networks," in *International Conference on Learning Representations*, 2020.

[18] P. Zhao, P.-Y. Chen, P. Das, K. N. Ramamurthy, and X. Lin, "Bridging mode connectivity in loss landscapes and adversarial robustness," *arXiv preprint arXiv:2005.00060*, 2020.

[19] D. Wu and Y. Wang, "Adversarial neuron pruning purifies backdoored deep models," *Advances in Neural Information Processing Systems*, vol. 34, pp. 16913–16925, 2021.

[20] K. Yoshida and T. Fujino, "Disabling backdoor and identifying poison data by using knowledge distillation in backdoor attacks on deep neural networks," in *Proceedings of the 13th ACM Workshop on Artificial Intelligence and Security*, 2020, pp. 117–127.

[21] H. Chen, C. Fu, J. Zhao, and F. Koushanfar, "Deepinspect: A black-box trojan detection and mitigation framework for deep neural networks," in *IJCAI*, vol. 2, no. 5, 2019, p. 8.

[22] X. Qiao, Y. Yang, and H. Li, "Defending neural backdoors via generative distribution modeling," *Advances in neural information processing systems*, vol. 32, 2019.

[23] X. Chen, C. Liu, B. Li, K. Lu, and D. Song, "Targeted backdoor attacks on deep learning systems using data poisoning," *arXiv preprint arXiv:1712.05526*, 2017.

[24] B. Wang, Y. Yao, S. Shan, H. Li, B. Viswanath, H. Zheng, and B. Y. Zhao, "Neural cleanse: Identifying and mitigating backdoor attacks in neural networks," in *2019 IEEE Symposium on Security and Privacy (SP)*. IEEE, 2019, pp. 707–723.

[25] S. Kolouri, A. Saha, H. Pirsiavash, and H. Hoffmann, "Universal litmus patterns: Revealing backdoor attacks in cnns," in *Proceedings of the IEEE/CVF Conference on Computer Vision and Pattern Recognition*, 2020, pp. 301–310.

[26] B. Chen, W. Carvalho, N. Baracaldo, H. Ludwig, B. Edwards, T. Lee, I. Molloy, and B. Srivastava, "Detecting backdoor attacks on deep neural networks by activation clustering," in *SafeAI@ AAAI*, 2019.

[27] N. Peri, N. Gupta, W. R. Huang, L. Fowl, C. Zhu, S. Feizi, T. Goldstein, and J. P. Dickerson, "Deep k-nn defense against clean-label data poisoning attacks," in *European Conference on Computer Vision*. Springer, 2020, pp. 55–70.

[28] B. Tran, J. Li, and A. Madry, "Spectral signatures in backdoor attacks," in *Proceedings of the 32nd International Conference on Neural Information Processing Systems*, 2018, pp. 8011–8021.

[29] A. Ilyas, S. Santurkar, D. Tsipras, L. Engstrom, B. Tran, and A. Madry, "Adversarial examples are not bugs, they are features," *arXiv preprint arXiv:1905.02175*, 2019.

[30] S.-M. Moosavi-Dezfooli, A. Fawzi, O. Fawzi, and P. Frossard, "Universal adversarial perturbations," in *Proceedings of the IEEE conference on computer vision and pattern recognition*, 2017, pp. 1765–1773.

[31] K. R. Mopuri, A. Ganeshan, and R. V. Babu, "Generalizable data-free objective for crafting universal adversarial perturbations," *IEEE transactions on pattern analysis and machine intelligence*, vol. 41, no. 10, pp. 2452–2465, 2018.

[32] S. Thys, W. Van Ranst, and T. Goedemé, "Fooling automated surveillance cameras: adversarial patches to attack person detection," in *Proceedings of the IEEE/CVF conference on computer vision and pattern recognition workshops*, 2019, pp. 0–0.

[33] F. Tramèr, A. Kurakin, N. Papernot, I. Goodfellow, D. Boneh, and P. McDaniel, "Ensemble adversarial training: Attacks and defenses," *arXiv preprint arXiv:1705.07204*, 2017.

[34] A. Athalye, N. Carlini, and D. Wagner, "Obfuscated gradients give a false sense of security: Circumventing defenses to adversarial examples," in *International conference on machine learning*. PMLR, 2018, pp. 274–283.

[35] Y. Dong, Q.-A. Fu, X. Yang, T. Pang, H. Su, Z. Xiao, and J. Zhu, "Benchmarking adversarial robustness on image classification," in *Proceedings of the IEEE/CVF Conference on Computer Vision and Pattern Recognition*, 2020, pp. 321–331.

[36] G. S. Dhillon, K. Azizzadenesheli, Z. C. Lipton, J. D. Bernstein, J. Kossaifi, A. Khanna, and A. Anandkumar, "Stochastic activation pruning for robust adversarial defense," in *International Conference on Learning Representations*, 2018.

[37] R. Shao, Z. Shi, J. Yi, P.-Y. Chen, and C.-J. Hsieh, "On the adversarial robustness of vision transformers," *arXiv preprint arXiv:2103.15670*, 2021.

[38] J. Cohen, E. Rosenfeld, and Z. Kolter, "Certified adversarial robustness via randomized smoothing," in *Proceedings of the 36th International Conference on Machine Learning*, ser. Proceedings of Machine Learning Research, K. Chaudhuri and R. Salakhutdinov, Eds., vol. 97. PMLR, 09–15 Jun 2019, pp. 1310–1320.

[39] A. Shafahi, M. Najibi, M. A. Ghiasi, Z. Xu, J. Dickerson, C. Studer, L. S. Davis, G. Taylor, and T. Goldstein, "Adversarial training for free!" in *Advances in Neural Information Processing Systems*. Curran Associates, Inc., 2019.

[40] L. Schmidt, S. Santurkar, D. Tsipras, K. Talwar, and A. Madry, "Adversarially robust generalization requires more data," in *Advances in Neural Information Processing Systems*, 2018.

[41] A. Madry, A. Makelov, L. Schmidt, D. Tsipras, and A. Vladu, "Towards deep learning models resistant to adversarial attacks," in *International Conference on Learning Representations*, 2018.

[42] S. Shan, E. Wenger, B. Wang, B. Li, H. Zheng, and B. Y. Zhao, "Using honeypots to catch adversarial attacks on neural networks," *arXiv*, 2019.

[43] A. Krizhevsky *et al.*, "Learning multiple layers of features from tiny images," 2009.

[44] J. Stallkamp, M. Schlipsing, J. Salmen, and C. Igel, "Man vs. computer: Benchmarking machine learning algorithms for traffic sign recognition," *Neural networks*, vol. 32, pp. 323–332, 2012.

[45] S. Zagoruyko and N. Komodakis, "Wide residual networks," in *British Machine Vision Conference 2016*. British Machine Vision Association, 2016.

[46] K. He, X. Zhang, S. Ren, and J. Sun, "Identity mappings in deep residual networks," in *Proceedings of the IEEE conference on computer vision and pattern recognition*, 2016.

[47] J. Deng, W. Dong, R. Socher, L.-J. Li, K. Li, and L. Fei-Fei, "Imagenet: A large-scale hierarchical image database," in *2009 IEEE conference on computer vision and pattern recognition*. Ieee, 2009, pp. 248–255.

[48] T. R. TaeJun Moon, "pytorch-tiny-imagenet," <https://github.com/tjmoon0104/pytorch-tiny-imagenet>.